

# Numerical modeling of black holes as sources of gravitational waves in a nutshell

Sascha Husa<sup>a</sup>

Institute for Theoretical Physics, University of Jena

**Abstract.** These notes summarize basic concepts underlying numerical relativity and in particular the numerical modeling of black hole dynamics as a source of gravitational waves. Main topics are the 3+1 decomposition of general relativity, the concept of a well-posed initial value problem, the construction of initial data for general relativity, trapped surfaces and gravitational waves. Also, a brief summary is given of recent progress regarding the numerical evolution of black hole binary systems.

## 1 Introduction

The theory of general relativity (GR) has enchanted generations of physicists through its conceptual and mathematical beauty, which is expressed in the simplicity and geometric nature of the Einstein equations,

$$G_{ab} = 8\pi\kappa T_{ab},$$

relating the curvature of spacetime to its matter content. It is in particular the connection of physical concepts such as the equivalence principle to a geometric description of nature, which is stressed in introductions to the field. General relativity makes many exciting physical predictions, such as the big bang, black holes, or gravitational waves. The theory also provides a seemingly inexhaustible supply of mathematical challenges, and many deep mathematical insights have been gained in trying to understand the physical content of the Einstein equations, such as the positive mass theorem [1] or the nonlinear stability of Minkowski space [2]. The currently emerging fields of gravitational wave astronomy, or, more generally, general relativistic astrophysics, are however changing this picture on a rapid timescale. A large international effort is underway to establish a network of gravitational wave detectors, such as LIGO [3,4], GEO [5,6] and VIRGO [7], some of which are already taking data at design sensitivity, and first publications have set new upper limits on the radiation from several sources (see *e.g.* [8,9,10]).

The field where the contact between mainstream general relativity and new applications is perhaps most intense, is numerical relativity (NR). Here one tries to systematically explore the solution space of the Einstein equations with numerical methods. One of the most advertised goals is to model the inspiral and collision of two black holes, and the resulting gravitational wave signals, in order to provide templates for gravitational wave data analysis. Many other applications are no less

---

<sup>a</sup> e-mail: [sascha.husa@gmail.com](mailto:sascha.husa@gmail.com)

exciting, *e.g.* the study of cosmological singularities (*i.e.* the predictions of general relativity about the very early universe), or critical collapse, where one probes the regime of extremely high curvatures created from the collapse of matter fields, *i.e.* a regime where classical general relativity will ultimately lose its validity and quantum effects will play a role.

While one of the most timely challenges for numerical relativity is the establishment of a “data analysis pipeline”, connecting analytical calculations of the early inspiral phase with numerical simulations and gravitational wave searches in actual detector data, on a technical level such simulations lead to challenging questions not only regarding the physics of general relativity, but also in applied mathematics, high performance computing and software engineering.

In order to set up reliable and efficient algorithms that predict detector signals from “first principles”-type numerical solutions of the Einstein equations it is essential that the individual steps are clearly understood, and subtleties or open issues be made transparent. Already the concept of gravitational wave emission from some source is highly nontrivial in general relativity, and touches upon the global structure of spacetimes. Setting up the Einstein equations as an initial value problem and solving them numerically raises several new problems in the theory of partial differential equations and their numerical solution. The complexity of the Einstein equations requires a sophisticated approach toward writing software in order to produce reliable results. Efficiency is paramount, when one actually aims to make the connection to data analysis, where large parameter studies are expected to be required. Understanding optimal choices in this regard requires a careful analysis of the interplay of the continuum equations, numerical methods and their implementation on current generations of high performance computing equipment.

A key idea when one wants to study the solutions of the Einstein equations in a systematic way, is to write the Einstein equations in the form of a well posed initial value problem. That this is possible, is not trivial, and an important test of the theory. Like the other fundamental theories of interactions (the electroweak interaction and quantum chromo-dynamics), general relativity can be interpreted as a gauge theory (in this case of the diffeomorphism group), and initial value formulations thus contain constraint equations. These constraint equations, which are associated with the diffeomorphism invariance, and the general subtleties of diffeomorphism invariance, like the absence of a fixed spacetime background which is essential in most areas of physics, create challenging problems for the mathematical treatment of the classical theory, its quantization, and for any treatment with approximation methods, such as numerical simulations. In a sense, the root of the problems to quantize gravity, is the same as for many problems to solve the Einstein equations numerically.

Discretizing GR can be approached in very different ways:

- One approach, that also has found applications in quantum gravity, is the direct discretization of the geometry (*e.g.* in Regge calculus [11]).
- A related idea is to use “discrete differential forms”, in analogy of a very successful method in electromagnetism, see *e.g.* [12].
- The mainstream approach, which I will follow in these notes, is to view the Einstein equations as a standard PDE (partial differential equations) problem.

All of the approaches however share the fundamental problem that due to the presence of the rather complicated constraints we have no direct access to physical degrees of freedom. As a consequence approximate solutions of constrained systems may not manifestly satisfy the constraints, it turns out that exponential drift off the constraint surface is typical, as is illustrated by the Maxwell example of eq. (9). It is possible to trade evolution equations for constraints when constructing the solution – a minimal number of (hyperbolic) evolution equations would correspond

to the local degrees of freedom (*i.e.* two for vacuum gravity). This may improve the quality of numerical evolutions, but there is no guarantee: since there are more equations than evolution variables, one still needs to worry whether the evolution equations that are not used to construct the solution will be (manifestly) satisfied.

The good news for numerical relativity is of course that in contrast to perturbation techniques numerical simulations do not rely on the smallness of physically relevant parameters, and can thus be applied in very general situations. Carefully crafted numerical simulations provide error estimates and convergence results. A particular challenge for the field, for instance, is to clarify the range of validity of post-Newtonian (PN) expansions [13], and significant progress has been made in this direction [14,15,16,17,18].

## 2 Gravitational Waves

Like electromagnetism, general relativity predicts waves: aspherically accelerated masses emit gravitational radiation. Both Maxwell's and Einstein's theories have two local degrees of freedom, which correspond to the two polarization states of waves in the theory. While in electromagnetism waves carry no monopole moment, in relativity there are no monopoles *and* no dipoles, to leading order wave emission is thus quadrupolar.

Under “everyday conditions”, including the conditions in a gravitational wave detector, the amplitude of gravitational waves is extremely small, and it is sufficient to consider the linearized theory. Consider the approximation  $g_{ab} = \eta_{ab} + h_{ab}$  for weak gravitational fields, where  $\eta_{ab}$  is the metric of Minkowski spacetime, and  $h_{ab}$  is a small perturbation. Using the definition

$$\bar{h}_{ab} = h_{ab} - \frac{1}{2}\eta_{ab}h^c{}_c$$

one can show that

$$\square \bar{h}_{ab} = 0$$

if the gauge condition

$$\partial \bar{h}_{ab} / \partial x^b = 0$$

is satisfied. The tensor  $\bar{h}_{ab}$  thus satisfies the standard wave equation on a flat background. It can be shown that a further gauge condition can be adopted to also set the trace of  $h_{ab}$  to zero,  $\eta^{ab}\bar{h}_{ab} = 0$ . In this “transverse-traceless (TT) gauge”, the metric perturbation  $h_{ab}$  corresponding to a wave traveling in the  $z$ -direction of a Cartesian coordinate system can be written as a linear combination of two polarizations  $h_+$  and  $h_\times$ :

$$h_{ij} = h_+(\mathbf{e}_+)_{ij} + h_\times(\mathbf{e}_\times)_{ij}, \quad (1)$$

where  $\mathbf{e}_{+,\times}$  are the basis tensors

$$(\mathbf{e}_+)_{ij} = \hat{x}_i\hat{x}_j - \hat{y}_i\hat{y}_j, \quad \text{and} \quad (\mathbf{e}_\times)_{ij} = \hat{x}_i\hat{y}_j + \hat{y}_j\hat{x}_i, \quad (2)$$

and  $\hat{x}$  and  $\hat{y}$  are the unit vectors in the  $x$  and  $y$  directions respectively. For an extensive introduction to the linearized theory of gravitational wave, including the principles of their detection, see [19].

When modeling sources of gravitational waves in full general relativity, it turns out that a notion of gravitational waves becomes highly nontrivial: because of diffeomorphism invariance there is no background spacetime available, on which gravitational waves can be defined in an unambiguous way. Such a definition is only

possible asymptotically for isolated systems. When the geometry “flattens out” to approach Minkowski spacetime at large distance from the sources, then Minkowski spacetime can be used as a suitable background, see sec. 5.

The weak field approximation can also be used to compute the radiation from sources, *e.g.* accelerated bodies. For velocities  $v \ll c$  and for wavelengths  $\lambda$  much larger than the size of the system, a weak field calculation yields the loss of energy of a system of massive bodies as

$$\frac{dE}{dt} = -\frac{G}{5c^5} \sum_{i,j} \left( \frac{d^3 Q_{ij}}{dt^3} \right)^2 \quad (3)$$

with  $Q_{ij} = \int \varrho (x_i x_j - \frac{1}{3} \delta_{ij} r^2) d^3 x$  is the mass quadrupole moment. Eq. (3) is known as the quadrupole formula (for the energy loss of the system). The radiation power scales with the sixth power of the frequency of the system. Due to the weakness of gravity, expressed in the factor  $\frac{G}{5c^5}$ , thus only systems of astrophysical dimensions – large masses moving at a significant fraction of the speed of light – generate significant amounts of gravitational radiation. While the motion of the earth around the sun only generates around 200 Watt of gravitational radiation, a close neutron star binary (100 km separation, 100 Hz) would generate approximately  $10^{45}$  Watt. In the inspiral and collision of two black holes, approximately 4 % of the total energy is radiated away in the form of gravitational waves – for the collision of two stellar size black holes with ten solar masses each, this would already be around 0.8 solar masses! Indirect confirmation of the predictions of general relativity for the energy loss of a binary system due to the emission of gravitational wave has been possible by measuring the tightening of the orbit of the Hulse-Taylor binary pulsar [20,21].

Two essential properties of gravitational waves for astrophysical observations are that they are not shielded by interstellar masses, and that detectors are sensitive to amplitude rather than intensity. The first means that not only will gravitational wave observations render possible the direct observation of phenomena that have not been observable so far, but we will also be able to see regions that have been hidden behind dust clouds. Gravitational waves represent the bulk motion of fast compact objects instead of incoherent superposition of many atoms, which is typical of electromagnetic observations. The observation of coherent wave trains makes gravitational wave observations similar to detecting sound waves, rather than to producing images, and in particular results in a direct sensitivity to amplitude. Consequently the sensitivity scales with  $1/\text{distance}$  instead of  $1/\text{distance}^2$  as for electromagnetic observations. This makes it much easier to observe objects at extreme distances, and also means that any improvement in detector sensitivity by some factor  $\lambda$  yields a factor  $\lambda^3$  in event rates.

### 3 The Initial Value Problem for General Relativity

#### 3.1 The Maxwell Equations

GR is a classical relativistic field theory much like Maxwell’s theory of electromagnetism, but it is nonlinear, and its dynamics involves the very structure of spacetime itself. We first discuss the structure of the Maxwell equations as an example. The Maxwell equations can be elegantly and geometrically formulated in a 4-dimensional way as

$$dF = 0, \quad d * F = 4\pi * J, \quad (4)$$

where  $F$  is the Faraday tensor of electromagnetic field strengths, and  $J$  is the 4-dimensional current. For practical purposes it is useful to solve the Maxwell equations as an initial value problem, that is to specify suitable data at some instant

of time, and then evolve them to the future. The formulation as an initial value problem allows a systematic approach to constructing solutions: First one needs to classify permissible initial data, then the future and/or past development of such data is determined uniquely by evolution equations. The Maxwell equations (4) are not written in this form, in particular it is not immediately obvious what permissible initial data would be, and whether time evolution of such data prescribes a unique solution.

A standard way to proceed is to prescribe a foliation of spacetime, *e.g.* by specifying a time function  $t(x^\mu)$ , such that the surfaces  $\Sigma_t$ , defined by  $t = \text{const.}$ , form a 1-parameter foliation of spacelike surfaces. One can then perform a geometric split of 4-dimensional tensorial quantities into 3-dimensional objects (*i.e.* objects defined in the tangent and co-tangent space of  $\Sigma_t$ ), and consider the equations for these 3-dimensional objects. It will prove useful to define a timelike unit normal to the surfaces  $\Sigma_t$ ,

$$n_a := \frac{\nabla_a t}{\sqrt{g^{ct} \nabla_c t}}.$$

The timelike unit normal can be used to define projection operators onto timelike (vertical) and spacelike (horizontal) directions. It is easy to check that  $n^a n_b$  projects onto the direction of the timelike unit normal, and the induced metric

$$h_{ab} = g_{ab} + n_a n_b \quad (5)$$

projects onto the tangent space of the spacelike hypersurface  $\Sigma_t$ , where  $g_{ab}$  denotes the (Lorentzian) spacetime metric, and  $h_{ab}$  then is the induced Riemannian (positive definite) metric on  $\Sigma_t$ . A covariant derivative  $D_a$  on  $\Sigma_t$  that is compatible with the metric  $h_{ab}$ ,  $D_a h_{bc} = 0$ , can be defined as

$$D_c T_{b_1 \dots b_s}^{a_1 \dots a_r} := h_c^{c'} h_{a'_1}^{a_1} \dots h_{a'_r}^{a_r} h_{b_1}^{b'_1} \dots h_{b_s}^{b'_s} \nabla_{c'} T_{b'_1 \dots b'_s}^{a'_1 \dots a'_r}.$$

Excellent pedagogical discussions of this geometric splitting procedure can be found in [22,23].

For the Maxwell equations one can now define

$$E^a = F_{ab} n^b, \quad B^e = \frac{1}{2} F_{cd} h^c{}_a h^d{}_b \epsilon^{abef} n_f,$$

the electric and magnetic field as projections of the field strength tensor  $F_{ab}$ , as well as the charge density  $\rho = J^a n_a$  and current  $j_b = J^a h_{ab}$ . On Minkowski spacetime, and also using the standard slices of Minkowski spacetime, the Maxwell equations separate into the following two groups of equations in terms of the electric and magnetic fields:

$$D_a E^a = 4\pi \rho, \quad D_a B^a = 0, \quad (6)$$

and

$$\partial_t E^a = \epsilon_{abc} \partial^b B^c - 4\pi j_a, \quad (7)$$

$$\partial_t B^a = -\epsilon_{abc} \partial^b E^c. \quad (8)$$

Since Eqs. (6) do not contain time derivatives, they have to be interpreted as constraint equations that restrict the space of allowed initial data, while (7,8) are evolution equations. It is not hard to show that if the constraints are satisfied initially, they will be satisfied for all times, furthermore, the evolution equations determine the time evolution in a unique way. Without these two facts, the initial value description of the Maxwell equations, eqs. (6-8) would make little sense. Because of

their linearity, the discussion of the initial value problem, and the solution of the constraints are tremendously simpler for the Maxwell equations than for the Einstein equations, but the essential structure is the same. Some remarks are in order: Counting degrees of freedom in eqs. (6-8), we find that there are 2 local degrees of freedom (6 first order evolution equations minus 2 constraint equations makes 4 first order in time or 2 second order in time equations), these correspond to the two polarization states of the electromagnetic field. It is clear that while for the continuum solution the constraints propagate (they are satisfied at all times by virtue of the evolution equations if they are satisfied at the initial time), this is not necessarily true for a numerical implementation. Discretization error may give rise to a growth in the constraints, which may lead to instability or at least spoil the physical validity of the approximate solution. We will see that the same problem appears for the Einstein equations. In electromagnetism, many approaches have been developed to deal with this issue, see [24] for a comparison. The most standard approach uses a formulation of the Maxwell equations in differential forms language, and directly translates the differential forms concepts to the discrete level [25]. This way, the constraints can be solved manifestly in the discrete problem.

The problems of preserving the constraints of the Maxwell theory become more pronounced in curved spacetime, and already in curved slices of Minkowski spacetime, where the constraint propagation equations become

$$\mathcal{L}_n D_i E^i = -K D_i E^i, \quad \mathcal{L}_n D_i B^i = -K D_i E^i \quad (9)$$

where  $\mathcal{L}_n$  is the Lie derivative along the timelike unit normal of the hypersurface, and  $K = D_a n^a$  is the trace of the extrinsic curvature of the hypersurface (see below). Here the sign of  $K$  is chosen such that  $K > 0$  corresponds to expansion, and  $K < 0$  to collapse. Clearly, in the collapsing case, initial violations of the constraints will be amplified. While a simple redefinition of the fields (densitizing them) solves the problem in the Maxwell case [26], this still provides a valuable toy model for similar problems in numerical relativity [27].

### 3.2 The Einstein Equations

The Einstein equations  $G_{ab} = 8\pi\kappa T_{ab}$  can be written as an initial value problem in formal analogy with the previous discussion of the Maxwell equations. There is much freedom in how to do this, and the route we will take is to very briefly introduce the most traditional way, and then to discuss its issues with regard to numerical relativity.

First, we need to make a careful choice of the topology of our spacetime manifold  $M$ , since the Einstein equations allow solutions that violate causality in a global way, *i.e.* geometries where there exists no spatial hypersurface  $\Sigma_t$  that uniquely determines the geometry at all earlier and later times. A necessary requirement for causality [23] is that the topology of the spacetime be  $\Sigma \times I$ , where  $\Sigma$  is a three-dimensional manifold, and  $I$  is a (possibly infinite) interval. We can then choose coordinates such that the line element takes the form

$$ds^2 = -\alpha^2 dt^2 + \gamma_{ab}(dx^a + \beta^a dt)(dx^b + \beta^b dt). \quad (10)$$

In particular we have thereby singled out a time function  $t$ .

We can now write the Einstein equations in terms of 3-dimensional objects: the induced metric  $h_{ab}$  (the definition in (10) coincides with the definition (5)), the shift vector  $\beta^a$  and the lapse function  $\alpha$ . The coordinate basis vector  $(\partial/\partial t)^a$  can be written in terms of the unit normal  $n^a$ , and the lapse and shift as

$$\left(\frac{\partial}{\partial t}\right)^a = \alpha n^a + \beta^a, \quad n^a \beta_a = 0.$$

A reduction to first order in time of the field equations can be obtained by introducing the extrinsic curvature (or second fundamental form)

$$K_{ab} := \frac{1}{2} \mathcal{L}_n \gamma_{ab} = \frac{1}{2\alpha} (\dot{\gamma}_{ab} - D_a \beta_b - D_b \beta_a), \quad (11)$$

$\mathcal{L}_n$  is again the Lie derivative with respect to the vector field  $n^a$ . Making a particular choice of adding constraints to the evolution equations one arrives at a “standard form” of the 3+1-decomposed Einstein equations, which has dominated numerical relativity for several decades, and is commonly referred to as the ADM-equations, and called the York-ADM equations here, since these equations can be viewed as a variant [28] of an evolution system discussed by Arnowitt, Deser and Misner in [29]:

$$D_b K^b_a - D_a K^b_b = 0, \quad {}^3R + (K^a_a)^2 - K_{ab} K^{ab} = 0, \quad (12)$$

$$\dot{K}_{ab} = -D_a D_b \alpha + \beta^c D_c K_{ab} + K_{cb} D_a \beta^c - K_{bc} D_a \beta^c + \alpha({}^3R_{ab} + K_c^c K_{ab}), \quad (13)$$

where for simplicity matter terms have been set to zero. The first two equations can be interpreted as constraints analogous to the Maxwell divergence constraints, while the third equation together with the definition of the extrinsic curvature (11) forms a first order in time evolution system. The Bianchi identity  $\nabla^a G_{ab} = 0$  implies that the constraints propagate, that is they are satisfied by virtue of the evolution equations at all times if they are satisfied initially. For a much more detailed discussion of the 3+1 decomposition of the Einstein equations see [30].

The big advantage of the ADM equations is their *relative* simplicity. The problem for numerical relativity, which has only been realized after several decades, is that the “free evolution problem”, where the constraints are only solved initially and only the evolution equations are used to construct the solution at later time, is only weakly hyperbolic in the language of hyperbolic partial differential equations, and the initial value problem therefore ill-posed (with the exception of certain subclasses of initial data such as spherical symmetry, which has added further to the confusion). The issue is discussed in detail in [31].

### 3.3 BSSN: the workhorse formulation for the binary black hole problem

For a long time, the standard choice of variables for writing the Einstein equations was based on the York-ADM equations [32]. It is known now, however, that the hyperbolic subsystem thus obtained is not well posed; specifically, it leads to a weakly hyperbolic set of equations (see *e.g.* [31]). A formidable industry of creating improved evolution systems has produced numerous alternatives, the most popular being the “BSSN family” [33,34,35]. This formulation is characterized by introducing a contracted connection term as a new variable, a conformal decomposition of the metric and extrinsic curvature variables, and adding constraints to the evolution equations.

Detailed discussions of well-posedness for the BSSN family have been given by Gundlach and Martin-Garcia [36,37,38]. The set of evolved variables are the conformally rescaled unimodular three-metric  $\tilde{\gamma}_{ij}$ , the logarithm of the conformal factor  $\phi$ , the trace of the extrinsic curvature  $K$ , the conformally rescaled traceless

extrinsic curvature  $\tilde{A}_{ij}$ , and the contracted Christoffel symbols  $\tilde{\Gamma}^i$ :

$$\phi = \frac{1}{12} \log(\det \gamma_{ij}), \quad (14)$$

$$\tilde{\gamma}_{ij} = e^{-4\phi} \gamma_{ij}, \quad (15)$$

$$K = \gamma^{ij} K_{ij}, \quad (16)$$

$$\tilde{A}_{ij} = e^{-4\phi} (K_{ij} - \frac{1}{3} \gamma_{ij} K), \quad (17)$$

$$\tilde{\Gamma}^i = \tilde{\Gamma}_{jk}^i \tilde{\gamma}^{jk}. \quad (18)$$

As is usual, we will adopt the convention that indices of densitized quantities (denoted with a tilde) are raised and lowered with the conformally rescaled three-metric  $\tilde{\gamma}_{ij}$ . The introduction of new variables leads to new constraints, one differential and two algebraic:

$$\mathcal{G} = \tilde{\Gamma}^i - \tilde{\gamma}^{jk} \tilde{\Gamma}_{jk}^i = 0, \quad \mathcal{S} = \det \gamma_{ij} - 1 = 0, \quad \mathcal{A} = \tilde{A}_i^i = 0, \quad (19)$$

which are again propagated by the evolution equations.

The standard Hamiltonian and momentum constraints of general relativity take the form [39]

$$\begin{aligned} \mathcal{H} &= e^{-4\phi} \left( \tilde{R} - 8\tilde{D}^j \tilde{D}_j \phi - 8(\tilde{D}^j \phi)(\tilde{D}_j \phi) \right) + \frac{2}{3} K^2 - \tilde{A}_{ij} \tilde{A}^{ij} - \frac{2}{3} \mathcal{A} K, \\ \mathcal{M}_i &= 6\tilde{A}^j_i (\tilde{D}_j \phi) - 2\mathcal{A}(\tilde{D}_i \phi) - \frac{2}{3} (\tilde{D}_i K) + \tilde{\gamma}^{kj} (\tilde{D}_j \tilde{A}_{ki}). \end{aligned}$$

The BSSN evolution equations, which are obtained from the Einstein equations by using the definitions (14) and making a standard choice for adding constraints, become

$$\begin{aligned} \mathcal{L}_n \phi &= -\frac{\alpha K}{6}, \\ \mathcal{L}_n \tilde{\gamma}_{ij} &= -2\alpha \tilde{A}_{ij}, \\ \mathcal{L}_n K &= -D^i D_i \alpha + \alpha \tilde{A}_{ij} \tilde{A}^{ij} + \frac{\alpha K^2}{3}, \\ \mathcal{L}_n \tilde{A}_{ij} &= -e^{-4\phi} (D_i D_j \alpha)^{TF} + \alpha \left( e^{-4\phi} (R_{ij})^{TF} + K \tilde{A}_{ij} - 2\tilde{A}_{ik} \tilde{A}^k_j \right), \\ \mathcal{L}_n \tilde{\Gamma}^i &= -2(\partial_j \alpha) \tilde{A}^{ij} + 2\alpha (\tilde{\Gamma}_{jk}^i \tilde{A}^{kj} - \frac{2}{3} \tilde{\gamma}^{ij} (\partial_j K) + 6\tilde{A}^{ij} (\partial_j \phi)), \end{aligned}$$

where  $\tilde{D}_i$  is covariant derivative associated with  $\tilde{\gamma}_{ij}$ ,  $\mathcal{L}_n = \partial_t - \mathcal{L}_\beta$  is the Lie derivative along the unit normal,  $T_{ij}^{TF}$  denotes the trace-free part of a tensor  $T_{ij}$ . The Ricci curvature in terms of the BSSN variables takes the form

$$\begin{aligned} R_{ij} &= -2\tilde{D}_i \tilde{D}_j \phi - 2\tilde{\gamma}_{ij} \tilde{D}^k \tilde{D}_k \phi + 4(\tilde{D}_i \phi)(\tilde{D}_j \phi) - 4\tilde{\gamma}_{ij} (\tilde{D}^k \phi)(\tilde{D}_k \phi), \\ &\quad - (1/2) \tilde{\gamma}^{lk} \partial_l \partial_k \tilde{\gamma}_{ij} + \tilde{\gamma}_{k(i} \partial_{j)} \tilde{\Gamma}^k + \tilde{\Gamma}^k \tilde{\Gamma}_{(ij)k} + 2\tilde{\gamma}^{lm} \tilde{\Gamma}_{l(i}^k \tilde{\Gamma}_{j)km} + \tilde{\gamma}^{lm} \tilde{\Gamma}_{im}^k \tilde{\Gamma}_{klj}. \end{aligned}$$

The algebraic constraints are typically solved at every time step, *e.g.* by setting  $\tilde{\gamma}_{ij} \rightarrow \tilde{\gamma}_{ij} \det \tilde{\gamma}^{-1/3}$  and  $\tilde{A}_{ij} \rightarrow \tilde{A}_{ij} - \frac{1}{3} \tilde{A}_{lm} \tilde{\gamma}^{lm} \tilde{\gamma}^{ij}$ .

Currently, the standard choice for evolving the lapse function for BSSN-evolutions is given by the so-called Bona-Masso family of slicing conditions:

$$\partial_t \alpha = -\alpha K f(\alpha), \quad (20)$$



in particular the choices  $f = 1$ , corresponding to harmonic time slicing, and  $f = 2/\alpha$ , which is usually termed “1+log” slicing, see [40].

In order to obtain long-term stable numerical simulations, it is equally important to construct a suitable shift vector field  $\beta^i$ . Here we report on evolutions where we evolve the shift vector according to a Gamma-freezing prescription [40]. A key feature of this particular choice is to drive the dynamics of the variable  $\tilde{\Gamma}^i$  towards a stationary state. As a “side effect” this choice creates a coordinate motion that drags the black holes along an inspiral orbit. A crucial effect of this method is that the resulting coordinate motion which corresponds to the naive physical intuition reduces artificial distortions in the geometry, which otherwise could easily trigger instabilities.

In summary, the solution procedure for the equations is as follows. First, we specify free data motivated by quasi-equilibrium arguments, then solve the 9 components of the constraint equations  $(\mathcal{H}, \mathcal{M}_i, \mathcal{G}^i, \mathcal{A}, \mathcal{S})$  to obtain initial data for the 17 evolution variables  $(\phi, \tilde{\gamma}_{ij}, K, \tilde{A}_{ij}, \tilde{\Gamma}^i)$ . The evolution system is completed by specifying evolution equations for the four gauge quantities  $(\alpha, \beta^i)$ , which yields a hyperbolic system that is second order in space and first order in time, and which determines the evolution of all 21 components of the “state vector” describing the geometry of spacetime.

In finite difference codes for the solution of nonlinear hyperbolic equations, it is common practice to add artificial dissipation terms to all right-hand-sides of the time evolution equations, schematically written as

$$\partial_t \mathbf{u} \rightarrow \partial_t \mathbf{u} + Q\mathbf{u}. \quad (21)$$

Such terms damp out high-frequency noise, *e.g.* as produced by mesh-refinement boundaries, and can be necessary to guarantee numerical stability for nonlinear problems [41]. The typical form of this terms is the Kreiss–Oliger dissipation operator [41] ( $Q$ ) of order  $2r$

$$Q = \sigma(-h)^{2r-1}(D_+)^r \rho(D_-)^r / 2^{2r}, \quad (22)$$

for a  $2r - 2$  accurate scheme, with  $\sigma$  a parameter regulating the strength of the dissipation, and  $\rho$  a weight function that we typically set to unity.

Discretization in space is performed with standard second-, fourth- [42,43] or sixth-order [44] accurate stencils. In particular, symmetric stencils are used, with the exception of the advection terms associated with the shift vector, asymmetric upwind stencils are used. Time integration is performed by standard Runge-Kutta type methods, in particular 3rd and 4th order Runge-Kutta and second order accurate three-step iterative Crank-Nicholson integrators as described in [31], where Courant limits and stability properties are discussed for the types of equations used here.

#### 4 Partial differential equations: Well-posedness and numerical stability for initial value problems

An excellent and seemingly trivial starting point for a discussion of numerical approximations is the model problem  $F(x, y) = 0$ . An important issue in the context of approximations is the sensitivity in the dependence of a solution  $y$  on an input parameter  $x$ . It is useful to define a *condition number*, which quantifies the worst possible effect on  $y$  when  $x$  is perturbed. Consider the perturbed eq.  $F(x + \delta x, y + \delta y) = 0$ , and define

$$K = \sup_{\delta x} \frac{||\delta y||/||y||}{||\delta x||/||x||}.$$

If  $K$  is small we call the problem well conditioned, if  $K$  is large ill conditioned, and if  $K(y) = \infty$  ill-posed or unstable. As a starting point for numerical relativity we clearly need the continuum problem to be well-conditioned – in GR this is far from trivial, *e.g.* because this will rely on a judicious choice of coordinate gauge.

We call an evolution problem well posed if a unique solution exists (in a gauge theory such as general relativity this requires a gauge choice) and depends continuously on the initial data. The latter condition is usually expressed as the condition

$$\|u(t)\| \leq K e^{a t} \|u(0)\|, \quad (23)$$

where the exponential term ensures robustness with respect to lower order terms, and the constants  $a$  and  $K$  can be chosen independently of the initial data. Note that this condition is only required local in time, since global in time solutions may not exist in a nonlinear theory – singularities may form! An obvious crucial question is which norm  $\|\cdot\|$  is appropriate for defining well-posedness of a certain type of differential equation. It turns out that for first order in space and time systems the standard  $L_2$ -norm is sufficient. Since the Einstein equations take the form of second differential order equations in the metric, a complete reduction to first order may seem artificial. Note that there is an important difference between first order reductions in space and in time: Reduction to first order in time leads to new evolution equations, but reduction to first order in space leads to new evolution *and* constraint equations. This enlargement of the phase space may not only reduce computational efficiency, but can also give rise to instabilities or pathologies not inherent in the original problem.

First order in time formulations provide a “normal form” for ordinary differential equations and are thus also convenient for systems of PDEs, which in numerical analysis are often discussed in terms of the “method of lines”. In this approach first only space is discretized, and time left continuous. PDEs are thus converted to coupled systems of ordinary differential equations. From a physical point of view, first order in time formulations are attractive, *e.g.* because they are most easily integrated into a Hamiltonian formulation.

The concept of well-posedness translates straightforwardly to the concept of numerical stability for discrete iterative problems. Consider a simple stable iterative algorithm

$$v^{n+1} = Q(t_n, v^n) v^n : \quad \|v^n\| \leq K e^{\alpha t_n} \|v^0\| \quad \forall v^0,$$

where  $v$  the solution vector and  $Q$  a matrix. The stability criterion allows  $e^{\alpha t_n}$  growth, but excludes  $e^{\alpha n}$  growth, *i.e.* for differential equations exponential growth is allowed in the continuum problem, but resolution dependent growth of the numerical algorithm is excluded.

To illustrate the analysis of numerical stability for a simple ODE problem, consider the standard textbook example

$$y' = \lambda y, \quad y(0) = y_0$$

and solve numerically with the forward Euler algorithm,

$$y_{n+1} = y_n + h y'_n = y_n + h \lambda y_n.$$

The stability criterion yields  $|y_{n+1}|/|y_n| = |1 + h\lambda|$ , and the algorithm is unstable for  $h > -2/\lambda$ . For  $\lambda > 0$  the continuum solution grows exponentially and even stable algorithms will suffer from ill-conditioning.

#### 4.1 The wave equation as a toy model for hyperbolic equations

The wave equation provides a standard example to illustrate well-posedness for evolution equations and to introduce different notions of the associated technical

concept of *hyperbolicity*. Starting with the second order form in 1D,  $\phi_{,tt} = c^2 \phi_{,xx}$ , we can obtain a mixed first/second order version,

$$\phi_{,t} = c\pi, \quad \pi_{,t} = c\phi_{,xx}$$

or a complete first order reduction

$$\phi_{,t} = c\pi, \quad \phi_{,x} = \psi, \quad \pi_{,t} = c\psi_{,x}, \quad \psi_{,t} = c\pi_{,x},$$

where  $\phi_{,x} = \psi$  now plays the role of a constraint which is preserved by the evolution equations:

$$\partial_t(\phi_{,x} - \psi) = \partial_x \partial_t \phi - \partial_t \psi = \partial_x \pi - \partial_x \pi = 0.$$

Note that the evolution equation for  $\phi$  decouples, and we may focus on the system of equations for  $\pi$  and  $\psi$ , which has the form

$$\partial_t u = A \partial_x u, \quad u = \{\pi, \psi\}, \quad A = \begin{pmatrix} 0 & c \\ c & 0 \end{pmatrix}.$$

We call the matrix  $A$ , or generally the coefficients of the highest spatial derivatives, the *principal part* of the system of partial differential equations. The characteristic variables  $v_{\pm} = \psi \pm \pi$  correspond to the eigenvectors of  $A$  and therefore satisfy advection equations,  $\dot{u}_{\pm} = \pm c u_{,x}$ , where the eigenvalues of  $A$  are  $\pm c$ . We can easily construct the general solution in Fourier space:

$$\Pi_{\omega} = \Pi_0 \cos(ct\omega) + i\psi_0 \sin(ct\omega), \quad \psi_{\omega} = \psi_0 \cos(ct\omega) + i\Pi_0 \sin(ct\omega).$$

The norm  $\|u\|^2 = \int |\Pi|^2 + |\psi|^2$  can easily be checked to satisfy  $\|u(t)\| = \|u(0)\|$ , well-posedness can thus directly be read off from the general solution, and numerical stability can be discussed in an analogous way. General theorems can be used to show stability against perturbations with lower order terms [45].

The system with principal part

$$A' = \begin{pmatrix} 1 & 1 \\ 0 & 1 \end{pmatrix}, \tag{24}$$

which we also will refer to as the 1-Jordan Block model, shows very different features:  $A'$  has real eigenvalues  $-(1, 1)$ , but does not have a complete set of eigenvectors (characteristics) and can not be diagonalized. The solution is  $U_{\omega} = (u, v)$ ,  $u = \omega t \sin \omega(t+x)$ ,  $v = \sin \omega(t+x)$ . Consider data with  $u(0) = 0$  and frequency  $\omega$  – in terms of the  $L_2$  norm we now get

$$\frac{\|U(t)\|}{\|U(0)\|} = \sqrt{1 + t^2 \omega^2}, \tag{25}$$

which does not satisfy our criterion for well-posedness. It turns out, that alternative norms can be chosen which render this problem well posed, but generic lower order perturbations convert the frequency dependent linear growth to frequency dependent exponential growth [45]. The choice of an appropriate norm is thus a subtle problem, and robustness with respect to lower order terms a crucial criterion.

## 4.2 First order systems

Consider a linear first order system with constant coefficients:

$$\dot{u} = A \partial_x u + Bu + C,$$

where  $u$  is interpreted as a multi-component object. It is easy to see that for a single equation, the function  $A$  corresponds to the propagation speed of the wave. For a system of equations, the eigenvalues of the matrix  $A$  clearly can again be interpreted as propagation speeds if the matrix  $A$  is diagonalizable. The eigenvectors are then called the characteristic variables. General theorems allow to restrict analysis of well-posedness and stability to  $B = C = 0$  [45]. The formal solution in Fourier space is

$$\dot{\hat{u}} = I\omega A \hat{u} \rightarrow \hat{u} = e^{I\omega A t} \hat{u}_0.$$

In order to study whether the solutions can be bounded by initial data and thus whether the system of equations allows a well-posed initial value problem, we need to evaluate  $e^{I\omega A}$ . Intuitively, no problems will arise if  $A$  is diagonalizable with real eigenvalues, the solution will then be purely oscillatory.

Well-posedness and stability can indeed be discussed in terms of eigenvalues (characteristic speeds) and eigenvectors (characteristic variables) of  $A$ , (again we refer to [45] for an excellent textbook presentation):

- If all eigenvalues (speeds) are real, the system is called (weakly) hyperbolic, and is well posed in absence of lower order terms in an appropriate norm.
- If a complete set of eigenvectors exists (the characteristic variables span the solution space), the system is called strongly hyperbolic, and admits a well posed initial value problem.
- If the system is strongly hyperbolic and admits a conserved energy it is called symmetrizable (symmetric) hyperbolic (strongly hyperbolic implies symmetrizable in 1D).

As an example consider the York-ADM equations (11,12,13) in 1D with lapse function  $\alpha = \sqrt{\det g}$  (a standard choice), linearized around Minkowski space:

$$\begin{aligned} \dot{h}_{ii} &= 2K_{ii} , \\ \dot{K}_{xx} &= \frac{1}{2}\partial_{xx}h_{xx} + \partial_{xx}(h_{yy} + h_{zz}) , \\ \dot{K}_{jj} &= \frac{1}{2}\partial_{xx}h_{jj} \quad (j = y, z) . \end{aligned}$$

Computing the Jordan normal form of the matrix  $A$  characterizing the principal part of the first order system yields

$$J(A) = \begin{pmatrix} 0 & 0 & 0 & 0 & 0 & 0 & 0 \\ 0 & -1 & 0 & 0 & 0 & 0 & 0 \\ 0 & 0 & -1 & 1 & 0 & 0 & 0 \\ 0 & 0 & 0 & -1 & 0 & 0 & 0 \\ 0 & 0 & 0 & 0 & 1 & 0 & 0 \\ 0 & 0 & 0 & 0 & 0 & 1 & 1 \\ 0 & 0 & 0 & 0 & 0 & 0 & 1 \end{pmatrix} .$$

All characteristic speeds are real, but there are 2 Jordan blocks, the eigenvectors of the characteristic matrix thus do not span the solution space and the system is only weakly hyperbolic. Nevertheless, many physics results have been obtained with the York-ADM system in spherical symmetry, and excellent test results are obtained in the 1D test suites of [46]. This is explained by noting that decoupling the  $xx$  components from the  $yy$  and  $zz$  components leads to well-posed systems and good numerical results. This happens for the “gauge wave” metric eq. (26), a linearized wave on flat background:

$$ds^2 = -dt^2 + dx^2 + (1+b)dy^2 + (1-b)dz^2, \quad b = A \sin\left(\frac{2\pi(x-t)}{d}\right),$$

but also in spherical symmetry, where again the  $yy$  and  $zz$  components (or, say  $\vartheta\vartheta$  and  $\varphi\varphi$ ) of the metric are not independent.

### 4.3 Second order in space, first order in time systems

First order in time, second order in space systems are typically used in astrophysically oriented numerical relativity codes, because of their simplicity and a vague expectation of better accuracy than first order reductions, which has at least partially been confirmed in [31]. Such systems are also attractive because they arise rather naturally in a Hamiltonian context. The issue of well-posedness for such systems has however only been clarified very recently [47,48,49,50,38,31], for much of the history of NR it was widely believed that a clean route to well-posedness requires the standard theory of first order hyperbolic systems, see *e.g.* [45] for an excellent textbook reference.

Again, the wave equation provides an excellent simple example of what is going on. The first order in time, second order in space wave equation is

$$\partial_t \phi(t, x) = \Pi(t, x), \quad \partial_t \Pi(t, x) = \partial_{xx} \phi(t, x).$$

Consider the family of solutions [51]

$$\phi(x, t) = \sin(\omega x) \cos(\omega t), \quad \Pi(x, t) = -\omega \sin(\omega x) \sin(\omega t)$$

with initial data  $\phi_0(x) = \sin(\omega x)$ ,  $\Pi_0(x) = 0$ . Varying  $\omega$  in the initial data, the  $L_2$  norm of the solution at time  $t$ ,  $\int_0^{2\pi} (|\phi|^2 + |\Pi|^2) dx$ , can be made arbitrarily large with respect to the initial data (whose norm is independent of  $\omega$ ), this contradicts well-posedness in  $L_2$ . Since numerical codes implementing these ill-posed equations, as well as the York-ADM evolution equations (13) which had been argued to lead to an ill-posed initial value problem before, did not show blowup, it was suggested [51] that well-posedness may not be crucial for numerical relativity codes.

The issue is resolved as follows: since all the solutions for the wave equation are actually bounded and show no growth, ill-posedness in  $L_2$  is not a sign of pathology in this case – the problem rather is the inappropriate use of the  $L_2$ -norm. Translating the first order norm that one gets from introducing

$$X = \partial_x \phi,$$

which leads to a well posed, symmetric hyperbolic problem, to the second order variables, and using the norm implied by this translation

$$\int_0^{2\pi} (|\Pi|^2 + |\partial_x \phi|^2) dx$$

does in fact yield well-posedness, as can be shown by pseudo-differential reduction (*i.e.* solving explicitly in Fourier-space) [47]. Note that on the discrete level an ambiguity regarding the discrete norm needs to be resolved: it is not clear how the derivative should be discretized, or whether this matters at all. This ambiguity is resolved in [31], see below. The reason that a code that implements the first order in time, second order in space wave equation does not show any pathological behavior is thus simple: the system is well posed, and as shown in [31] can be discretized stably in a straightforward way. The York-ADM equations are however indeed only weakly hyperbolic and therefore lead to an ill-posed initial value problem. However, the growth is only linear, and is easily dismissed without careful convergence tests, or when artificial dissipation is added. Using the norm that would correspond to a first order-reduction of the system notions of well-posedness and hyperbolicity can then indeed be defined for mixed order hyperbolic systems [47,48,49,50,31].

A simple “normal form” for mixed order hyperbolic systems has been introduced in [31]:

$$\partial_t \mathbf{u} = P \mathbf{u}, \quad \mathbf{u} = \begin{pmatrix} u \\ v \end{pmatrix}, \quad P = \begin{pmatrix} A^i \partial_i + B & C \\ D^{ij} \partial_i \partial_j + E^i \partial_i + F & G^i \partial_i + J \end{pmatrix}.$$

Evolved variables are split into two types:  $u$  are differentiated twice and  $v$  are not. Not all second order in space systems can be written in this form (a simple example is the heat equation,  $u_t = u_{xx}$ , which is parabolic). Now consider the *second order principal symbol*  $\hat{P}'$  and a matrix  $E$ , which is the principal part of the associated first order system:

$$\hat{P}' = \begin{pmatrix} i\omega A^n & C \\ -\omega^2 D^{nn} & i\omega G^n \end{pmatrix}, \quad \hat{E} = i\omega \begin{pmatrix} 0 & 0 & 0 \\ 0 & A^n & C \\ 0 & D^{nn} & G^n \end{pmatrix}.$$

The main result on the continuum level of the equations is that if  $E$  is diagonalizable in a regular way, the initial value problem is well posed:

$$\|\mathbf{u}(t, \cdot)\| \leq K e^{\alpha t} \|\mathbf{u}(0, \cdot)\|, \quad \|\mathbf{u}\|^2 \equiv \int |u|^2 + \sum_{i=1}^d |\partial_i u|^2 + |v|^2 d^d x,$$

where the norm is again the straightforward translation of the  $L^2$  norm of the associated first order system. This result is equivalent to results that had previously been obtained by other authors in [47,49,37]. The result may seem trivial, but has ended a long controversy in numerical relativity about whether the evolution systems typically used in mainstream numerical relativity are well posed, or even whether their well-posedness can be discussed in a mathematically rigorous way. Recent results along the lines sketched here prove well-posedness results for the evolution systems and coordinate gauge conditions that are actually used in large scale binary black hole evolutions [52], which had seemed far out of reach only a few years ago.

The appropriate norm for the discrete case is

$$\|\cdot\| \rightarrow \|\mathbf{u}\|_{h,D_+}^2 \equiv \|u\|_h^2 + \|v\|_h^2 + \sum_{i=1}^d \|D_{\pm i} u\|_h^2.$$

The ambiguity of discretizing the derivative in the norm is resolved by using the first order forward ( $D_+$ ) or backward ( $D_-$ ) spatial derivative in combination with standard centered second or fourth order differencing. Using centered derivatives in the norm is shown not to be robust with regard to perturbations in lower order terms.

Note that for the continuum version of the matrix  $E$  the frequency  $\omega$  can be factored out, which is not generally the case for the discrete version of  $E$ , this would only hold in general if the second derivative is really also the derivative of the first derivative on the discrete level. For some evolution systems in general relativity certain standard discretizations are thus problematic, as discussed in [31].

#### 4.4 Stable and well-posed is not enough

Clearly, well-posedness and numerical stability are not sufficient to guarantee successful numerical simulations, since exponential growth or blowup in finite time,

which is allowed for well posed problems, is typically not tolerable for numerics (unless the timescale of the growth is sufficiently smaller than the timescale of interest in the solution). A typical trick to get rid of exponential growth is a change of variables, but this is in general difficult for tensors. As an example, it is a standard result of textbooks on ordinary differential equations that sufficiently regular ODE initial value problems are always well-posed, solutions may however blow up in finite time:

$$y' = \lambda y^2, y(0) = y_0 \quad \rightarrow \quad y(x) = y_0 / (x y_0 - 1).$$

In numerical relativity, exponential growth of the continuum solution already appears in seemingly trivial test problems. Consider a “gauge wave” metric – the flat metric of Minkowski space in coordinates that correspond to a traveling wave of coordinate distortion. This metric provides a challenging test for most evolution codes and is part of a numerical relativity test suite [46]:

$$ds^2 = -H dt^2 + H dx^2 + dy^2 + dz^2, \quad H = H(x - t) = 1 - A \sin\left(\frac{2\pi(x - t)}{d}\right). \quad (26)$$

This line element represents Minkowski spacetime with a nontrivial choice of harmonic time slicing ( $\nabla^a \nabla_a t = 0$ ). One analytic source of rapidly growing error is the instability of flat space on  $T^3$ . Another problem is the existence of a family of harmonic, exponential gauge modes corresponding to  $H \rightarrow e^{\lambda t} H$ , with arbitrary  $\lambda$ . This problem can be modeled by a nonlinear wave propagating on Minkowski space [53]:

$$\eta^{ab} \partial_a \partial_b \Phi - \frac{1}{\Phi} \eta^{ab} (\partial_a \Phi)(\partial_b \Phi) = 0 = \Phi \eta^{ab} \partial_a \partial_b \log \Phi.$$

Imposing periodic boundary conditions, one evolves on a 3-torus, *i.e.* there are no boundaries. For  $\Phi > 0$  the Cauchy problem is well-posed. In addition to the solution  $\Phi = 1 + F(t - z)$ ,  $F > -1$ , the system also admits the solutions

$$\Phi_\lambda = e^{\lambda t} (1 + F(t - z))$$

for arbitrary  $\lambda$ . Numerical errors will excite the growing modes, which eventually dominate the signal. As pointed out in [53], an obvious solution is to use  $\log \Phi$  as an evolution variable, but the example just models a situation that does arise in numerical relativity, where it is not clear how to take the logarithm of the metric.

For a problem that is actually ill-posed, the situation will be much worse than for our gauge-wave toy problem: typically higher frequencies will correspond to faster growth (*i.e.* larger  $a, K$  in the estimate (23)). Since better resolution of the grid does in particular allow higher frequencies, improving the resolution will in general lead to a numerical solution that grows faster. This is analogous to an unstable numerical scheme – in such a case, the discretized equations do not lead to a well posed problem.

## 5 Energy, momentum, and radiation

For astrophysical systems like stars or inspiraling black holes, it is physically reasonable to assume that spacetime becomes flat in the limit of large distance, and that the systems can be considered “isolated”, *i.e.* unaffected by the large scale structure of the universe. The formulation of a rigorous concept of “asymptotic flatness” in GR is far from straightforward, due to the absence of a background metric or preferred coordinate system, in terms of which falloff rates can be specified. There

are two possible routes to overcome this problem: In the first approach one simply assumes the existence of a suitable coordinate system, which is then used to formulate falloff conditions for tensor components in this coordinate system. We will follow this approach below to define quantities such as the total energy of a gravitating system. The obvious drawback is that taking limits is often problematic, in particular in a numerical context, and coordinate invariance of expressions has to be carefully checked. A resolution of these problems is provided by a definition of asymptotic flatness, where, after a suitable conformal rescaling of the metric, “points at infinity” are added to the manifold, one thus works on a compactified auxiliary manifold, and local differential geometry can be used to study the asymptotic properties of the gravitational field [54]. Note that the notion of asymptotic flatness at timelike infinity does not make much sense in a general situation, because then all energy would have to be radiated away, leaving only flat space behind – excluding black holes or “stars”. The important notions are asymptotic flatness in spacelike and null (lightlike) directions. A detailed discussion of the global structure of spacetimes describing isolated systems in general relativity is not really possible here – an excellent overview is given in the textbook [23], for work in the context of numerical relativity see *e.g.* [55,56,57,58,27].

The concept of asymptotic flatness of isolated systems is intimately related to the possibility of defining the total energy-momentum for such systems in general relativity. In GR there exists no known well-defined local energy density of the gravitational field, but a total energy-momentum, which transforms as a 4-vector under asymptotic Lorentz transformations, can be assigned to an isolated system [23], analogous to a particle in special relativity. It is a constant of motion and can therefore be expressed in terms of the initial data on an asymptotically flat Cauchy hypersurface.

If a manifold has more than one asymptotically flat end, *e.g.* in the presence of wormholes of the Einstein-Rosen-bridge type, then – in general different – masses can be associated with each of these asymptotic regions.

The expression for the energy momentum of GR at spatial infinity has been given first by Arnowitt, Deser and Misner in 1962 [29] in the context of the Hamiltonian formalism, and is usually called the ADM momentum, the time component being called the ADM energy or, somewhat inconsistently, the ADM mass, different from the rest mass to be defined below.

The expressions for the mass and momentum are given as limits of surface integrals over non-covariant quantities, and have to be evaluated in asymptotically Cartesian (regular) coordinates  $\{x^i\}$  – where the components of the metric tend to  $\text{diag}(1, 1, 1)$  for large radii  $r = \sqrt{x_i x^i}$ . The surfaces are spheres  $S_r$  of radius  $r$ .

We define the surface integrals (which we will also refer to as ADM integrals)

$$E(r) = \frac{1}{16\pi} \int_{S_r} \sqrt{g} g^{ij} g^{kl} (g_{ik,j} - g_{ij,k}) dS_l, \quad (27)$$

$$P_j(r) = \frac{1}{8\pi} \int_{S_r} \sqrt{g} (K_j^i - \delta_j^i K) dS_i, \quad (28)$$

$$J_j(r) = \frac{1}{8\pi} \epsilon_{jl}^m \int_{S_r} \sqrt{g} x^l (K_m^i - K \delta_m^i) dS_i \quad (29)$$

which have to be evaluated in an asymptotically Cartesian coordinate system.

The ADM energy  $M_{ADM}$  and linear and angular momentum  $P_j$  and  $J_j$  are then given by [59,28]

$$M_{ADM} = \lim_{r \rightarrow \infty} E(r), \quad P_j = \lim_{r \rightarrow \infty} P_j(r), \quad J_j = \lim_{r \rightarrow \infty} J_j(r), \quad (30)$$

and the rest mass  $M_R$  can be defined as  $M_R^2 = M_{ADM}^2 - \sum_{j=1,3} P_j P_j$ .



For an asymptotically Schwarzschildian metric  $h_{ab}$  (here the extrinsic curvature falls off faster than in the general case, which allows for a boost, *i.e.* linear momentum) the ADM mass can be read off directly as the  $\frac{1}{r}$ -term of the metric:

$$h_{ab} = \left(1 + \frac{m}{2r}\right)^4 \delta_{ab} + q_{ab}, \quad |q_{ab}| \leq \frac{\text{const.}}{1+r^2}. \quad (31)$$

A fundamental issue of GR is the positivity of the ADM energy, since if the energy of an isolated system can be negative, it would most likely be unstable and decay to lower and lower energies. While it is trivial to write down a metric with negative mass, for reasonable matter fields with nonnegative energy density (thus satisfying the dominant energy condition), nonnegativity of the ADM energy thus can be expected on physical grounds. Indeed a complete proof of this positive energy conjecture has been given in 1982 by Schoen & Yau [1] (several simplified proofs have been given afterwards).

For radiation processes we also require definitions of total energy, linear and angular momentum that decrease as energy and linear as well as angular momentum are radiated to infinity. The appropriate quantities are the Bondi quantities [60], which can be defined as taking the limit of the ADM integrals not toward spatial infinity, but rather toward null infinity [61,62,63], *i.e.*, the limit to infinite distance is taken for constant retarded time instead of on a fixed Cauchy slice. In the context of our numerical treatment, the ADM and Bondi quantities can be calculated by computing values at several radii, and then performing a Richardson extrapolation (in extraction radius, not, as is more usual, in grid spacing). Here the Bondi quantities can be computed at any time for a fixed extraction radius, and have to be compared between different radii by taking into account the light travel time between the timelike cylinders of different radii, see *e.g.* [43].

Radiation quantities are conveniently defined in terms of the (complex) Bondi news function  $\mathcal{N}(t) := \partial_t(h_+ - Ih_-)$ , which is the time derivative of the complex strain  $h$  taken at null infinity, where  $h_+$  and  $h_-$  are the two polarization modes of the gravitational field, see eq. (1). The expressions for the radiated energy and momenta then become

$$\frac{dE}{dt} = \frac{1}{16\pi} \int_{\Omega} \mathcal{N} \bar{\mathcal{N}} d\Omega, \quad (32)$$

$$\frac{dP_i}{dt} = -\frac{1}{16\pi} \int_{\Omega} \ell_i \mathcal{N} \bar{\mathcal{N}} d\Omega, \quad (33)$$

$$\frac{dJ_z}{dt} = -\frac{1}{16\pi} \text{Re} \left[ \int_{\Omega} \mathcal{N}_{,\phi} \left( \int_{-\infty}^t \bar{\mathcal{N}} d\hat{t} \right) d\Omega \right], \quad (34)$$

where

$$\ell_i = (-\sin\theta \cos\phi, -\sin\theta \sin\phi, -\cos\theta),$$

and an overbar denotes complex conjugation. The strain  $h$  is most often computed indirectly via double time integration of certain projections of the curvature tensor, see *e.g.* [43] for a detailed recent description in the context of numerical relativity.

## 6 Horizons

This section introduces the concept of trapped surfaces and apparent horizons. These are intimately related to two of the most fascinating features of general relativity: the appearance of singularities and the appearance of causal membranes:

event horizons that enclose so-called black holes – regions of spacetime that do not allow any information to escape to the outside world.

For quite some time it was not clear whether singularities, which have first been found in highly symmetrical spacetimes such as the Friedmann-Robertson-Walker cosmologies or the Schwarzschild spacetime, are really generic, or mere artifacts of the high symmetry in these situations. Only in 1965 the generic character of singularities has been proven in a theorem by Penrose [64]. A variety of similar theorems with modified assumptions has followed, for an overview see *e.g.* Hawking and Ellis [22] or Wald [23].

A crucial notion in the singularity theorems is that of a *trapped surface*: a space-like 2-surface with the property that the area of the outgoing wavefront *decreases* toward the future. The central idea of the singularity theorems is then, that provided some energy condition (*e.g.* that the local energy density of matter is nonnegative) holds for the matter fields, gravity is always attractive, and light rays always get focused. Thus, if a region of spacetime starts to collapse, as is signaled by the appearance of a trapped surface, this collapse cannot be halted and will continue until a spacetime singularity forms.

The original Penrose singularity theorem [64] states that, provided a closed trapped surface exists and the Cauchy surface is non-compact, at least one of the following things will happen:

1. There occurs negative local energy density.
2. Einstein’s equations are violated.
3. The spacetime manifold is incomplete – a singularity occurs.
4. The concept of spacetime loses its meaning at very high curvatures, possibly due to quantum gravity effects.

This means, that in the framework of classical general relativity a trapped surface signals the occurrence of a singularity in the future.

While the singularity theorems have shown that sufficiently “strong” initial data will develop a singularity, these theorems make no statement about the nature of the singularities. It is of particular interest, whether the singularities that arise in a physically reasonable collapse situation is visible to any observer.

A wide-spread hope – at least in classical general relativity – is expressed by the cosmic-censorship hypothesis of Penrose [65], which is by now floating through the literature in various formulations. The basic idea is that naked singularities – that is singularities that can be seen by outside observers – should not arise from regular initial data. The future light cone of the beginning of a naked singularity would be a Cauchy horizon and destroy predictability. A distinction is made between global and local nakedness. Globally naked singularities can influence asymptotic infinity (in an asymptotically flat setting) – they are not hidden by an event horizon. Inside of an event horizon, there may sit a locally naked singularity – while no information can escape from it to infinity it can still be seen by observers inside of the black hole. To rule out locally naked singularities all singularities have to be spacelike, which is equivalent to the spacetime being globally hyperbolic. In the weaker formulation, global hyperbolicity is only required outside of an event horizon.

Counter-examples to overly restrictive formulations of cosmic-censorship are known in various cases, *e.g.* for phenomenological matter like dust outside of the physical validity of the equation of state, but also for sets of measure zero in the space of initial data (related to a collection of phenomena known as “critical collapse”, see *e.g.* [66] for an extensive overview).

Black holes, although dangerous and exotic, from this viewpoint are the *good guys*, the *bad guys* are naked singularities. From the viewpoint of quantum gravity, a violation of cosmic censorship actually seems rather desirable, since then regions of

strong curvature, where quantum effects are important, may actually be observable in the outside world.

A notion that is derived from that of a trapped surface, is the *apparent horizon*: the boundary of the region of trapped surfaces, which turns out to be “marginally trapped” – *i.e.* the area of the outgoing wavefront neither increases nor decreases toward the future. In contrast to event horizons, which are defined in a global manner and can only be determined if the maximal time development is known, apparent horizons and trapped surfaces are defined locally in time, within a single slice, and can be directly determined from the initial data. Since the event horizon can only be defined if a suitable notion of infinity exists in a given spacetime, one could take the point of view of defining a black hole directly by means of apparent horizons [67]. The location in a given geometry and the analysis of the physical properties of the apparent horizon thus play an important role in numerical relativity. “Apparent horizon finders” are an essential component of all binary black hole evolution codes and discussed extensively in [68].

## 7 Initial data for numerical relativity

### 7.1 The conformal approach to solve the constraints

We have already taken a first step in identifying freely specifiable data for Einstein’s equations by formulating them as a Cauchy problem. Given appropriate initial data on a spacelike hypersurface, the spacetime is determined as a unique time development (modulo diffeomorphisms) of these data for future and past times. Due to the presence of the constraint equations (12) the initial data can not be specified freely, and the next task therefore is to extract the unconstrained part of the initial data in such a way that the constraints then uniquely determine the whole set of initial data, and thus the whole spacetime. There exists a standard formalism to accomplish this goal and solve the constraints, the conformal approach developed by Lichnerowicz, York, Ó Murchadha and others [69]. The conformal approach is based on conformal rescaling, in particular of the spatial metric  $h_{ab}$ , which is expressed from a ‘base metric’  $\bar{h}_{ab}$  and a conformal factor  $\psi$  as

$$h_{ab} = \psi^4 \bar{h}_{ab}, \quad \psi > 0. \quad (35)$$

By combination of (35) with a similar rescaling and decomposition of the extrinsic curvature into a traceless symmetric part and a part that is derived from a vector potential, the constraints will be written as a coupled set of four well posed quasilinear elliptic PDEs for four ‘gravitational potentials’.

For the conformal rescaling (35) the scalar curvature transforms as

$$R_h = \psi^{-5} (R_{\bar{h}} \psi - 8 \Delta_{\bar{h}} \psi).$$

Next we define the trace-free part of the extrinsic curvature by

$$A^{ab} := K^{ab} - \frac{1}{3} h^{ab} K.$$

The rescaling

$$A^{ab} = \psi^{10} \bar{A}^{ab} \quad (36)$$

then results in the property

$$D_a A^{ab} = \psi^{-10} \bar{D}_a \bar{A}^{ab}, \quad (37)$$

where  $\bar{D}_a$  is the unique derivative operator associated with the metric  $\bar{h}_{ab}$ . For  $K = \text{const.}$ , eq. (37) expresses the fact, that the momentum constraint is conformally invariant, if the tracefree part of the extrinsic curvature is properly rescaled. Note that the definition of  $A^{ab}$  in eq. (36) is equivalent to setting

$$A_{ab} = \psi^2 \bar{A}_{ab},$$

where

$$A_{ab} = A^{cd} h_{ac} h_{bd}, \quad \bar{A}_{ab} = \bar{A}^{cd} \bar{h}_{ac} \bar{h}_{bd}.$$

The traceless symmetric tensor  $\bar{A}^{ab}$  is decomposed as

$$\bar{A}^{ab} = \bar{A}_{TT}^{ab} + (LW)^{ab}$$

into a divergence-free (transverse) traceless part  $\bar{A}_{TT}^{ab}$  and a tracefree part that can be obtained from a potential  $W^a$ ,

$$(LW)^{ab} := \bar{D}^a W^b + \bar{D}^b W^a - \frac{2}{3} \bar{h}^{ab} \bar{D}^c W^c.$$

Insertion of the reverse decomposition

$$\bar{A}_{TT}^{ab} = \bar{A}^{ab} - (LW)^{ab}$$

into the constraint equations (12) yields

$$D_a (LW)^{ab} = -\bar{D}_a \bar{A}^{ab} + \frac{2}{3} \psi^6 D^b K + 8\pi \psi^{10} j^b, \quad (38)$$

$$-\Delta_{\bar{h}} \psi + \frac{1}{8} R_{\bar{h}} \psi - \frac{1}{8} \psi^{-7} (\bar{A}^{ab} - (LW)^{ab})^2 + \frac{1}{12} \psi^5 K^2 = 2\pi \psi^5 \rho, \quad (39)$$

where we have now kept the energy density  $\rho$  and momentum density  $j^b$  of matter fields in the expressions. The freely specifiable quantities here are the metric  $\bar{h}_{ab}$ , the trace of the extrinsic curvature,  $K$ , and a symmetric tracefree tensor  $\bar{A}^{ab}$ , which together comprise the local freedom in choosing initial data. The constraint equations now take the form of a coupled elliptic system of PDEs for the 'potentials'  $\psi$  and  $W^a$ , the initial data are reconstructed as

$$h_{ab} = \psi^4 \bar{h}_{ab}, \quad K^{ab} = (\bar{A}^{ab} - (LW)^{ab})^2 \psi^{-10} + \frac{1}{3} K \psi^{-4} h^{ab}.$$

Prior to the choice of a set of fields  $(\bar{h}_{ab}, K, \bar{A}^{ab})$ , one has to specify a 3-manifold  $S$ , on which the fields  $(\bar{h}_{ab}, K, \bar{A}^{ab})$  are defined and the equations (39,38) are to be solved. If the manifold  $S$  has a nonempty boundary, or is not compact, it will be necessary to impose boundary conditions or asymptotic falloff conditions, which have to be chosen, along with the topology of  $S$ , on physical grounds.

Due to the diffeomorphism invariance of GR, different initial data sets will give rise to the same spacetime (*e.g.* different slices of the same spacetime in different coordinate systems), which leads to the question for the number of local *physical* degrees of freedom represented by the initial data  $(\bar{h}_{ab}, K, \bar{A}^{ab})$ . Since  $(\bar{h}_{ab}$  and  $K^{ab})$  are both symmetric, the initial data are represented by 12 free functions. Three of these correspond to conditions on the spatial coordinate system (the metric  $\bar{h}_{ab}$  can be regarded as given by three functions by choosing a coordinate system where it is diagonal). In addition to initial data which are equivalent with respect to spatial diffeomorphisms, also data on different Cauchy surfaces may give rise to the same spacetime. A hypersurface is specified by one function, which can usefully be identified with the trace of the extrinsic curvature, also called the mean curvature –

since it corresponds to an average over the components of the extrinsic curvature. By imposing the 4 constraint equations on the remaining 8 free functions and dividing by two, one arrives at 2 local degrees of freedom per space point (confirming that GR is indeed a field theory). This is the same number of degrees of freedom as results from the linearized theory, which is the theory of a spin 2 field, where the 2 degrees of freedom can be identified with 2 independent states of polarization – just as in the case of electromagnetism (see *e.g.* ref. [23], sec. 4.4).

Most discussions of initial data restrict attention to so-called constant mean curvature (CMC) hypersurfaces. The condition that the mean curvature, or equivalently the trace of the extrinsic curvature, be constant is a coordinate independent statement and decouples the system (39,38). The procedure of solution then becomes the following:

1. Choose  $\bar{h}_{ab}, \bar{A}^{ab}, K = \text{const.}$ ,
2. solve (38) for  $K^{ab}$ ,
3. solve (39) for the scale factor  $\psi$ , regarding the extrinsic curvature term as source.

Slices with  $K = 0$  are called maximal slices. Maximal hypersurfaces embedded in a Lorentzian manifold locally maximize the 3-dimensional volume in the same way as a timelike geodesic maximizes the proper length, or a minimal 2-surface in Riemannian 3-space minimizes the area. The opposite extreme, *i.e.* a minimal 3-slice, or a maximal 2-surface is not possible, since deformations of the submanifold that just make the embedding 'more wiggly' will result in a change of volume of a definite sign: it is positive for a Riemannian hypersurface or a timelike curve in a Lorentzian manifold, and negative for a submanifold of a Riemannian manifold. The concept of extremal submanifolds thus is a natural generalization of geodesics as straightest curves.

Considering the fact, that even simple metrics can be made to look arbitrarily complicated by coordinate choice, it is natural to specify initial data on hypersurfaces that are embedded as simply as possible, which leads to the consideration of maximal (or more general CMC) slices as 'least wiggly'. Another advantage of maximal slices is that a foliation of maximal slices avoids singularities [70], which has been utilized in many numerical calculations.

Initial data for black holes can conveniently be constructed by "filling" the spacetime volume inside the horizon with artificial asymptotically flat ends. This construction enforces the presence of "throats" – minimal surfaces, and for non-vanishing extrinsic curvature also the presence of horizons (for vanishing extrinsic curvature the outermost minimal surfaces is actually an apparent horizon). These asymptotic regions are typically compactified for technical convenience, rendering the nontrivial topology of the resulting spacetime representable on  $R^3$ , or  $S^3$  if the physical asymptotically flat end is also compactified. Compactification naturally leads to singular behavior at the coordinate locations of the artificial asymptotic ends, which are commonly referred to as "punctures". The treatment of the singularity in the constraint equations is well understood [71]. The use of such initial data has first been advocated in [72], and has become the method of choice for a large fraction of work on binary black holes in numerical relativity following the prescription of Brandt and Brügmann [73]. The standard simplifying assumptions in the binary black hole literature are that the spatial geometry is conformally flat and that the extrinsic curvature is of the Bowen-York form [74], which is a family of solutions to the momentum constraint on a flat background, for which the total linear and angular momentum can be freely specified. By linearity of the momentum constraint and the flat background, superposition can be applied to construct multiple-black hole solutions. Removing the assumption of conformal flatness becomes an issue particularly for spinning black holes, see [75] for a recent discussion.

An essential question regarding the construction of initial data is the issue of physical validity of the initial data set, say for the inspiral of two black holes. Data sets should contain little or no “artificial radiation”, and should correspond to the actual inspiral of astrophysical compact objects. The typical aim is to start with initial data that correspond to the astrophysically most relevant case of quasi-circular inspiral, which essentially means that the orbital eccentricity is very small: eccentricity is radiated away rather efficiently for inspiraling black holes [76]. It has recently been possible for the nonspinning equal mass case to directly use the initial momenta (and separations) computed from a PN inspiral, and show that not only the eccentricity of such initial data is very small, but also that the influence of “artificial radiation” inherent in the initial data can essentially be neglected. I expect this method to carry over to more general scenarios, for large spins of the black holes non-conformally flat initial data might have to be used along the lines of [75] and the references cited therein. For extensive reviews of the problem of construction initial data for general relativity see [77,30].

## 8 The binary black hole revolution

The inspiral and collision of compact objects – in particular of black hole binary systems – is considered one of the most important sources of gravitational waves for earth- and space-based detectors. Producing templates for gravitational-wave data analysis that describe signals from inspiraling compact binaries will require large parameter studies, and correspondingly large computational resources: The eventual goal of our simulations is to map the physical parameter space of gravitational wave signals from black hole coalescence, which is essentially given by the mass ratio and individual spins, as well as the initial orientation of the spins. The latter determines in particular the spin orientation at merger time, which may have a significant influence on the gravitational wave signal.

In order to produce “complete” waveforms, which contain large numbers of gravitational wave cycles from the inspiral phase, as well as the merger and ringdown phases, it is necessary to start the numerical simulations in the regime where Post-Newtonian analytical calculations are valid. These describe very accurately the waveforms of the early inspiral process, but break down for small separations of the black holes. This “matching” of analytical and numerical results requires large initial black-hole separations and large integration times.

The numerical solution of the full Einstein equations represents a very complex problem, and for two black holes the spacetime singularities that are encountered in the interior of black holes pose an additional challenge. In order to obtain accurate results both the use of mesh refinement techniques *and* a good choice of coordinate gauge are essential. Together with the complicated structure of the equations — a typical code has between ten and several dozen evolution variables, and, when expanded, the right hand sides of the evolution equations have thousands of terms — this yields a computationally very complex and mathematically very subtle problem.

For a long time, typical runs had been severely limited by the achievable evolution time before the simulations became too inaccurate or before the computer code became unstable, and there were serious doubts whether numerical relativity techniques could produce gravitational-wave templates, at least in the near future. This picture has drastically changed ever since in spring of 2005 Pretorius [78] presented the first simulation lasting for several orbits, using adaptive mesh refinement, second-order finite differencing, a sophisticated method to excise the singular interior of the black hole from the grid, and an implicit evolution algorithm.

An alternative to the “excision” method of treating black holes is to “fill” the black hole with a topological defect in the form of an interior space-like asymp-

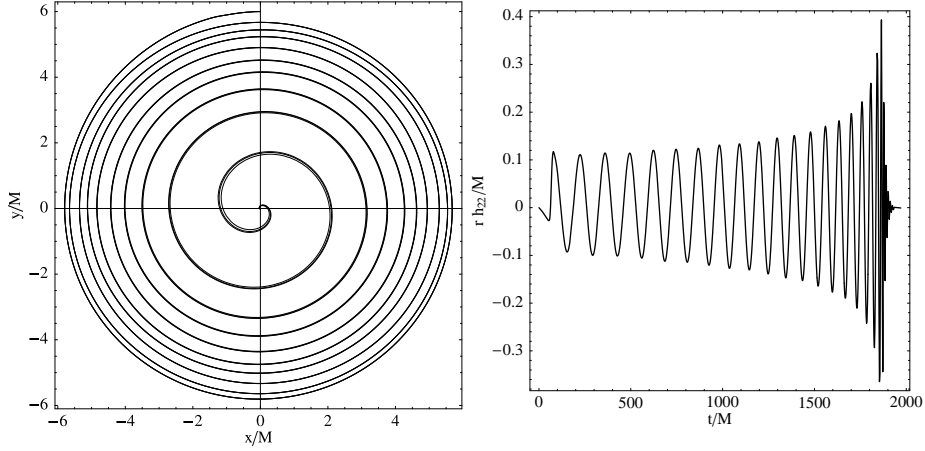


**Fig. 1.** Left panel: Coordinate tracks of the puncture location of one black hole for simulations with grid sizes of the innermost boxes of  $\{64^3, 72^3, 80^3\}$ , starting at a coordinate separation of  $D = 12M$ . Only in the last few orbits small differences are visible between the three runs discernable. Right panel: the waveform  $h_+$ , rescaled with the extraction radius. Figure taken from [92].

otic end, the “puncture” [73], and to freeze the evolution of the asymptotic region through a judicious choice of coordinate gauge [79,80,40]. The latter approach, combined with a setup where the topological defect is allowed to move across the grid (“moving puncture” approach [81,82]) has led to a giant leap forward in the field [83,84,85,86,87,88,89], taking the first orbit simulations of black holes [90,78] to more than ten orbits and allowing accurate wave extraction.

In order to overcome phase inaccuracies in long evolutions, spectral methods have been suggested and significant progress has been made by the Caltech-Cornell group [91]. The Jena group has recently obtained good results with 6th order accurate finite differencing methods [92], which has enabled us to perform highly accurate evolutions over nine orbits (see fig. (1) – units in the figures are given in units of the total initial black hole mass  $M$ ) and perform a detailed comparison with predictions from PN approximations [92,44,18]. For an extensive overview on PN approximations see [13].

A long standing problem has been the specification of non-eccentric initial data for numerical relativity simulations, which model inspiraling compact objects which have shed the eccentricity of their orbit through gravitational radiation. In [44] we show, that at least for the nonspinning equal mass case the initial momenta can be taken from a PN prescription. Part of the reason why this works is that the coordinate gauge used for numerical relativity agrees with the so-called ADMTT gauge adopted for PN calculations to excellent accuracy until very late in the inspiral, see fig. (3). The PN calculation is performed such that all initial eccentricity is shed during the first few hundred orbits, as shown in fig. (8).

A particular focus of the last few months has been the so-called recoil or rocket effect due to “beamed” emission of gravitational radiation [94,95,96]. By momentum conservation, radiation of energy in a preferred direction corresponds to a loss of linear momentum and the black hole that results from the merger thus recoils from the center-of-mass frame with speeds of up to several thousand km/s. The velocity of this “kick” depends on the configuration of the system (*e.g.* the mass ratios and spins) and details of the merger dynamics, but not on the total mass (velocity is dimensionless in geometric units).

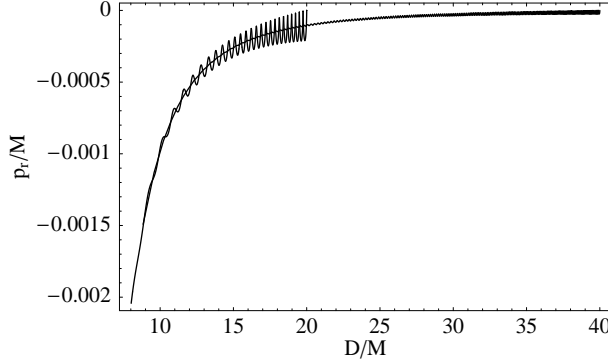


**Fig. 2.** The radial momentum component is plotted versus separation for PN-inspirals starting from  $D = 20M$  and  $D = 40M$ . A separation of  $D = 20M$  is clearly not sufficient to produce non-eccentric inspiral parameters, since small oscillations can still be seen at  $D = 11M$ , while for  $D = 40M$  the initial eccentricity has essentially decayed away. Figure taken from [44].

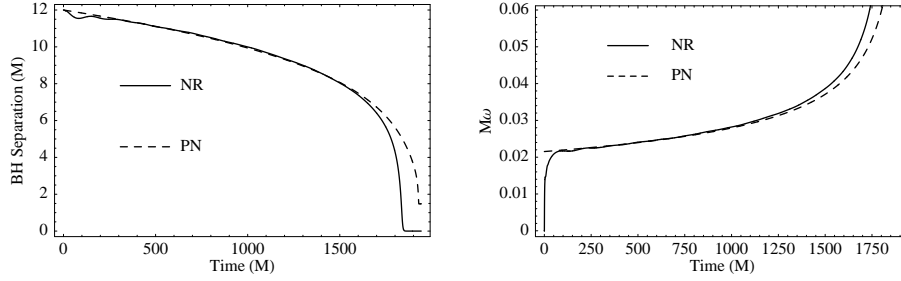


**Fig. 3.** Orbital coordinate motion of a 9-orbits numerical relativity evolution compared with a PN evolution with the same initial parameters. In both panels the PN evolution is drawn as a dashed line. Top panel: the separation of the black holes (the puncture position in the full NR case). Bottom panel: the coordinate angular velocity. Figure taken from [18].

From an astrophysical point of view, the recoil effect is particularly interesting for massive black holes with masses  $> 10^5 M_\odot$ , which exist at the center of many galaxies and may have a substantial impact on the structure and formation of their host galaxies. The largest recoil effects have so far been found [93,97] for a particularly simple configuration: equal mass black holes with (initially) anti-aligned spins in the orbital plane. Such large kicks are on the order of 1% of the speed of light, and larger than the escape velocity of about 2000 km/s of giant elliptical galaxies. Smaller but still significant kick velocities have been found for several different types of black hole configurations [98,99,100,101,102,103].

Many challenges remain in the binary black hole problem: extreme mass ratios, combined, say, with large spins may remain problematic for some time; incorporating realistic matter models adds a wealth of new problems. In order to perform large parameter studies, significant further optimizations for current codes are probably required, along with further mathematical insights and a better understanding of the general relativity aspects of the methodological foundations of the field. I believe that with the “binary black hole revolution” the field of numerical relativity



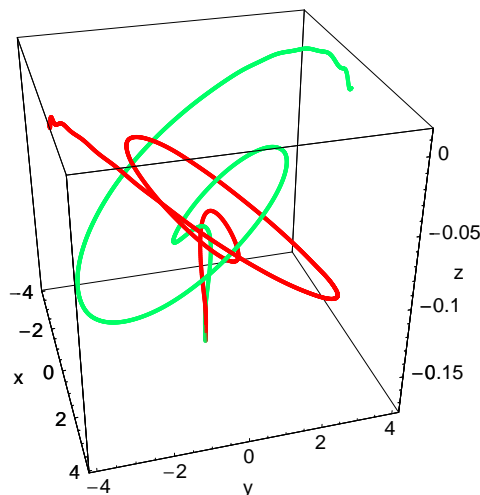


**Fig. 4.** Coordinate positions of the black-hole punctures for model MII from [93] up to  $t = 180$ . The black holes move out of the original plane and after merger the final black hole receives a kick in the negative  $z$ -direction. Figure taken from [93].

has found a new beginning rather than come to its end – and the study of colliding compact objects in particular will remain fruitful scientific ground for some time.

I am grateful to Mark Hannam, Norbert Lages and Christof Gattringer for reading the manuscript and identifying some misprints and unclear points.

## References

1. R. Schoen, S.T. Yau, *Commun. Math. Phys.* **65**, 45 (1979)
2. D. Christodoulou, S. Klainerman, *The Global Nonlinear Stability of the Minkowski Space* (Princeton University Press, Princeton, 1993)
3. A.A. Abramovici, W. Althouse, R.P. Drever, Y. Gursel, S. Kawamura, F. Raab, D. Shoemaker, L. Sievers, R. Spero, K.S. Thorne et al., *Science* **256**, 325 (1992)
4. LIGO, LIGO – <http://www.ligo.caltech.edu/>
5. K. Danzmann, *Lecture Notes in Physics* **410**, 184 (1992)
6. GEO, gEO600 – <http://www.geo600.uni-hannover.de/>
7. VIRGO, vIRGO – <http://www.virgo.infn.it/>
8. B. Abbott (LIGO Scientific) (2007), [arXiv:0704.3368](https://arxiv.org/abs/0704.3368) [gr-qc]
9. B. Abbott et al. (LIGO Scientific) (2007), [arXiv:0704.0943](https://arxiv.org/abs/0704.0943) [gr-qc]
10. B. Abbott et al. (LIGO Scientific) (2007), [gr-qc/0702039](https://arxiv.org/abs/gr-qc/0702039)
11. A.P. Gentle, *General Relativity and Gravitation* **34**, 1701 (2002), [gr-qc/0408006](https://arxiv.org/abs/gr-qc/0408006)
12. D.L. Meier, *Astrophys. J.* **595**, 980 (2003), [astro-ph/0312052](https://arxiv.org/abs/astro-ph/0312052)
13. L. Blanchet, *Living Rev. Relativity* **5**, 3 (2002), [gr-qc/0202016](https://arxiv.org/abs/gr-qc/0202016), <http://www.livingreviews.org/lrr-2002-3>
14. A. Buonanno, G.B. Cook, F. Pretorius (2006), [gr-qc/0610122](https://arxiv.org/abs/gr-qc/0610122), [gr-qc/0610122](https://arxiv.org/abs/gr-qc/0610122)
15. J.G. Baker, J.R. van Meter, S.T. McWilliams, J. Centrella, B.J. Kelly, *Phys. Rev. Lett.* **99**, 181101 (2007), [gr-qc/0612024](https://arxiv.org/abs/gr-qc/0612024)
16. E. Berti et al., *Phys. Rev.* **D76**, 064034 (2007), [gr-qc/0703053](https://arxiv.org/abs/gr-qc/0703053)
17. Y. Pan et al., *Phys. Rev.* **D77**, 024014 (2008), [0704.1964](https://arxiv.org/abs/0704.1964)

18. M. Hannam, S. Husa, J.A. González, U. Sperhake, B. Brügmann, *Phys. Rev. D* **77**, 044020 (2008), [arXiv:0706.1305 \[gr-qc\]](#)
19. E.E. Flanagan, S.A. Hughes, *New J. Phys.* **7**, 204 (2005), [gr-qc/0501041](#)
20. R. Hulse, J. Taylor, *Astrophys. J.* **195**, L51 (1975)
21. J.H. Taylor, J.M. Weisberg, *Astrophys. J.* **253**, 908 (1982)
22. S.W. Hawking, G.F.R. Ellis, *The large scale structure of spacetime* (Cambridge University Press, Cambridge, England, 1973), ISBN 0-521-09906-4
23. R.M. Wald, *General relativity* (The University of Chicago Press, Chicago, 1984), ISBN 0-226-87032-4 (hardcover), 0-226-87033-2 (paperback)
24. G. Toth, *J. Comput. Phys.* **161**, 605 (2000)
25. A. Bossavit, *Computational Electromagnetism* (Academic Press, Boston, USA, 1998)
26. L. Antón, O. Zanotti, J.A. Miralles, J.M. Martí, J.M. Ibáñez, J.A. Font, J.A. Pons, *Astrophys. J.* **637**, 296 (2006), [astro-ph/0506063](#)
27. S. Husa, C. Schneemann, T. Vogel, A. Zenginoglu (2005), to appear in Proceedings of the 2005 spanish relativity meeting, AIP Conference Proceedings, 8 pages., [gr-qc/0512033](#)
28. J.W. York, in *Sources of gravitational radiation*, edited by L.L. Smarr (Cambridge University Press, Cambridge, UK, 1979), pp. 83–126, ISBN 0-521-22778-X
29. R. Arnowitt, S. Deser, C.W. Misner, in *Gravitation: An introduction to current research*, edited by L. Witten (John Wiley, New York, 1962), pp. 227–265, [gr-qc/0405109](#)
30. E.ourgoulhon (2007), [gr-qc/0703035](#)
31. G. Calabrese, I. Hinder, S. Husa, *J. Comp. Phys.* **218**, 607 (2005), [gr-qc/0503056](#)
32. J.W. York, Jr., in *Sources of Gravitational Radiation*, edited by L.L. Smarr (Cambridge University Press, Cambridge, UK, 1979), pp. 83–126, ISBN 0-521-22778-X
33. T.W. Baumgarte, S.L. Shapiro, *Phys. Rev. D* **59**, 024007 (1998), [gr-qc/9810065](#)
34. M. Shibata, T. Nakamura, *Phys. Rev. D* **52**, 5428 (1995)
35. M. Alcubierre, B. Brügmann, T. Dramlitsch, J.A. Font, P. Papadopoulos, E. Seidel, N. Stergioulas, R. Takahashi, *Phys. Rev. D* **62**, 044034 (2000), [gr-qc/0003071](#)
36. C. Gundlach, J.M. Martin-Garcia, *Phys. Rev. D* **70**, 044032 (2004), [gr-qc/0403019](#)
37. C. Gundlach, J.M. Martin-Garcia, *Class. Quantum Grav.* **23**, S387 (2006), [gr-qc/0506037](#)
38. C. Gundlach, J.M. Martin-Garcia, *Phys. Rev. D* **74** (2006), [gr-qc/0604035](#)
39. H. aki Shinkai, G. Yoneda, *Progress in Astronomy and Astrophysics* (Nova Science, 2003), chap. Re-formulating the Einstein equations for stable numerical simulations: Formulation Problem in Numerical Relativity, [gr-qc/0209111](#)
40. M. Alcubierre, B. Brügmann, P. Diener, M. Koppitz, D. Pollney, E. Seidel, R. Takahashi, *Phys. Rev. D* **67**, 084023 (2003), [gr-qc/0206072](#)
41. H.O. Kreiss, J. Oliger, *Methods for the approximate solution of time dependent problems* (GARP publication series No. 10, Geneva, 1973)
42. Y. Zlochower, J.G. Baker, M. Campanelli, C.O. Lousto, *Phys. Rev. D* **72**, 024021 (2005), [gr-qc/0505055](#)
43. B. Brügmann, J.A. González, M. Hannam, S. Husa, U. Sperhake, W. Tichy, *Phys. Rev. D* **77**, 024027 (2008), [gr-qc/0610128](#)
44. S. Husa, M. Hannam, J.A. González, U. Sperhake, B. Brügmann, *Phys. Rev. D* (2007), [arXiv:0706.0904 \[gr-qc\]](#)
45. B. Gustafsson, H.O. Kreiss, J. Oliger, *Time dependent problems and difference methods* (Wiley, New York, 1995)
46. M. Alcubierre et al., *Class. Quantum Grav.* **21**(2), 589 (2004), [gr-qc/0305023](#)
47. G. Nagy, O.E. Ortiz, O.A. Reula, *Phys. Rev. D* **70**, 044012 (2004), [gr-qc/0402123](#)
48. H. Beyer, O. Sarbach, *Phys. Rev. D* **70**, 104004 (2004), [gr-qc/0406003](#)
49. C. Gundlach, J. Martin-Garcia, *Phys. Rev. D* **70**, 044031 (2004), [gr-qc/0402079](#)
50. C. Gundlach, J.M. Martín-García, *Phys. Rev. D* **70**, 044032 (2004), [gr-qc/0403019](#)
51. S. Frittelli, R. Gómez, *J. Math. Phys.* **41**, 5535 (2000), [<http://arXiv.org/abs/gr-qc/0006082>]
52. C. Gundlach, J.M. Martin-Garcia, *Phys. Rev. D* **74**, 024016 (2006), [gr-qc/0604035](#)

53. M.C. Babiuc, B. Szilágyi, J. Winicour, Lect. Notes Phys. **692**, 251 (2006), [gr-qc/0404092](#)
54. R. Penrose, Phys. Rev. Lett. **10**, 66 (1963)
55. J. Winicour, Living Rev. Relativity **1**, 5 (1998), [Online article], <http://www.livingreviews.org/lrr-1998-5>
56. S. Husa, *Numerical relativity with the conformal field equations*, in *Proceedings of the 2001 spanish relativity meeting*, edited by L. Fernández, L.M. González (Springer, 2003), Vol. 617 of *Lecture Notes in Physics*, pp. 159–192
57. L. Andersson, Lect. Notes Phys. **604**, 183 (2002), [gr-qc/0205083](#)
58. J. Frauendiener, Living Rev. Relativity **7**(1) (2004), <http://www.livingreviews.org/lrr-2004-1>
59. N. O’Murchadha, J.W. York, Phys. Rev. D **10**(8), 2345 (1974)
60. H. Bondi, M.G.J. van der Burg, A.W.K. Metzner, Proc. R. Soc. London **A269**, 21 (1962)
61. J.I. Katz, D. Lynden-Bell, W. Israel, Class. Quantum Grav. **5**, 971 (1988)
62. J.D. Brown, S.R. Lau, J. York, James W., Phys. Rev. D **55**, 1977 (1997), [gr-qc/9609057](#)
63. E. Poisson, *A Relativist’s Toolkit: The Mathematics of Black-Hole Mechanics* (Cambridge University Press, 2004), ISBN 0521830915
64. R. Penrose, Phys. Rev. Lett. **14**, 57 (1965)
65. R. Penrose, Riv. Nuovo Cimento **1**, 252 (1969)
66. C. Gundlach, Living Rev. Relativity **2**, 4 (1999), [gr-qc/0001046](#), <http://www.livingreviews.org/lrr-1999-4>
67. A. Ashtekar, B. Krishnan, Living Rev. Relativity **7**, 10 (2004), [gr-qc/0407042](#), <http://www.livingreviews.org/lrr-2004-10>
68. J. Thornburg, Living Rev. Relativity (2006), [Online article], [gr-qc/0512169](#)
69. Y. Choquet-Bruhat, J.W. York, Jr., in *Gen. Rel. Grav.*, edited by A. Held (Plenum, New York, 1980), Vol. 1, pp. 99–172
70. F. Estabrook, H. Wahlquist, S. Christensen, B. DeWitt, L. Smarr, E. Tsiang, Phys. Rev. D **7**(10), 2814 (1973)
71. S. Dain, Lect. Notes Phys. **604**, 161 (2002), [gr-qc/0203021](#)
72. R. Beig, N. O’Murchadha, Class. Quantum Grav. **11**, 419 (1994)
73. S. Brandt, B. Brügmann, Phys. Rev. Lett. **78**(19), 3606 (1997), [gr-qc/9703066](#)
74. J.M. Bowen, J.W. York, Phys. Rev. D **21**(8), 2047 (1980)
75. M. Hannam, S. Husa, B. Brügmann, J.A. Gonzalez, U. Sperhake, Class. Quantum Grav. **24**, S15 (2007), [arXiv:gr-qc/0612001](#)
76. P.C. Peters, Phys. Rev. **136**, B1224 (1964)
77. G.B. Cook, Living Rev. Relativity **3**, 5 (2000), <http://www.livingreviews.org/lrr-2000-5>
78. F. Pretorius, Phys. Rev. Lett. **95**, 121101 (2005), [gr-qc/0507014](#)
79. B. Brügmann, Int. J. Mod. Phys. D **8**, 85 (1999)
80. M. Alcubierre, B. Brügmann, Phys. Rev. D **63**, 104006 (2001), [gr-qc/0008067](#)
81. M. Campanelli, C.O. Lousto, P. Marronetti, Y. Zlochower, Phys. Rev. Lett. **96**, 111101 (2006), [gr-qc/0511048](#)
82. J.G. Baker, J. Centrella, D.I. Choi, M. Koppitz, J. van Meter, Phys. Rev. Lett. **96**, 111102 (2006), [gr-qc/0511103](#)
83. F. Herrmann, D. Shoemaker, P. Laguna (2006), [gr-qc/0601026](#)
84. M. Campanelli, C.O. Lousto, Y. Zlochower, Phys. Rev. D **73**, 061501(R) (2006), [gr-qc/0601091](#)
85. J.G. Baker, J. Centrella, D.I. Choi, M. Koppitz, J. van Meter, Phys. Rev. D **73**, 104002 (2006), [gr-qc/0602026](#)
86. J.G. Baker, J. Centrella, D.I. Choi, M. Koppitz, J. van Meter, M.C. Miller, Astrophys. J. **653**, L93 (2006), [astro-ph/0603204](#)
87. M. Campanelli, C.O. Lousto, Y. Zlochower, Phys. Rev. D **74**, 041501(R) (2006), [gr-qc/0604012](#)
88. U. Sperhake, Phys. Rev. **D76**, 104015 (2007), [gr-qc/0606079](#)

89. M. Hannam, S. Husa, D. Pollney, B. Brügmann, N. Ó Murchadha, Phys. Rev. Lett. **99**, 241102 (2007), [gr-qc/0606099](#)
90. B. Brügmann, W. Tichy, N. Jansen, Phys. Rev. Lett. **92**, 211101 (2004), [gr-qc/0312112](#)
91. M.A. Scheel, H.P. Pfeiffer, L. Lindblom, L.E. Kidder, O. Rinne, S.A. Teukolsky, Phys. Rev. D **74**, 104006 (2006), [gr-qc/0607056](#)
92. S. Husa, J.A. González, M. Hannam, B. Brügmann, U. Sperhake, Class. Quantum Grav. **25**, 105006 (2008), [arXiv:0706.0740 \[gr-qc\]](#)
93. J.A. González, M.D. Hannam, U. Sperhake, B. Brügmann, S. Husa, Phys. Rev. Lett. **98**(23), 231101 (2007), [gr-qc/0702052](#)
94. W.B. Bonnor, M.A. Rotenberg, Proc. R. Soc. Lond. A. **265**, 109 (1961)
95. A. Peres, Phys. Rev. **128**, 2471 (1962)
96. J.D. Bekenstein, Astrophys. J. **183**, 657 (1973)
97. M. Campanelli, C.O. Lousto, Y. Zlochower, D. Merritt, Phys. Rev. Lett. **98**, 231102 (2007), [gr-qc/0702133](#)
98. J.G. Baker, J. Centrella, D.I. Choi, M. Koppitz, J. van Meter, M.C. Miller, Astrophys. J (2007), [astro-ph/0603204](#)
99. F. Herrmann, I. Hinder, D. Shoemaker, P. Laguna, Class. Quantum Gravity **24**, S33 (2007)
100. J.A. González, U. Sperhake, B. Brügmann, M. Hannam, S. Husa, Phys. Rev. Lett. **98**, 091101 (2007), [gr-qc/0610154](#)
101. F. Herrmann, I. Hinder, D. Shoemaker, P. Laguna, R.A. Matzner (2007), [gr-qc/0701143](#)
102. M. Koppitz, D. Pollney, C. Reisswig, L. Rezzolla, J. Thornburg, P. Diener, E. Schnetter (2007), [gr-qc/0701163](#)
103. M. Campanelli, C.O. Lousto, Y. Zlochower, D. Merritt, Astrophys. J. **659**, L5 (2007), [gr-qc/0701164](#)